

A low power, on demand electrothermal valve for wireless drug delivery applications

Po-Ying Li,^a Tina K. Givrad,^b Roya Sheybani,^b Daniel P. Holschneider,^{bc} Jean-Michel I. Maarek^b and Ellis Meng^{*ab}

Received 27th May 2009, Accepted 2nd October 2009

First published as an Advance Article on the web 19th October 2009

DOI: 10.1039/b910248e

We present a low power, on demand Parylene MEMS electrothermal valve. A novel Ω -shaped thermal resistive element requires low power (\sim mW) and enables rapid valve opening (\sim ms). Using both finite element analysis and valve opening experiments, a robust resistive element design for improved valve opening performance in water was obtained. In addition, a thermistor, as an inrush current limiter, was added into the valve circuit to provide variable current ramping. Wireless activation of the valve using RF inductive power transfer was demonstrated.

Introduction

One-shot, disposable microvalves have been widely investigated for many microfluidic applications such as space exploration,¹ polymerase chain reaction (PCR),² lab-on-a-chip,^{3–5} and drug delivery.^{6,7} (Table 1). These valves utilize many activation methods to achieve valve opening and, among them, electrothermal activation is the most common strategy.^{2,5–7} Electrothermal valves usually consist of a temporary membrane (or plug) that blocks the flow path and a heater that melts the membrane to open the valve. Depending on the membrane materials used, power consumption can be as high as 2250 mW for a Pt/Ti membrane⁶ to 67 mW for a PMMA membrane.⁷ Other valve operation principles include smart alloys,¹ microspheres,⁴ and hydrogels.³

Generally, one-shot microvalves should have low power consumption, a short time constant, and reliability.⁸ In implantable drug delivery systems, low power consumption is critical; these systems rely on batteries or radio frequency (RF) coils for power. Activation of the valve occurs over a period referred to as the time constant⁹ and is highly dependent on the design. Devices with widely varying time constants, from \sim ms to \sim min, may be selected to suit a particular application. Reliable valve operation and performance are also important design requirements, especially in the case of implantable devices. Our application involves the use of a valve for gating radiotracer delivery in neuroimaging of small animals and requires a single-use, low power, on demand valve.

Previously, an implantable infusion pump system was investigated that was based on an alternative neuroimaging strategy to achieve real-time neuroimaging of rats.^{10,11} By triggering an off-the-shelf solenoid valve, pressurized radioactive tracer followed by euthanasia were rapidly infused into the systemic circulation.

Areas of elevated cerebral blood flow were immediately labeled and brains were collected, fixed, and imaged using autoradiography. Labeled regions correspond to high activity areas linked to the particular behavior being studied. Thus, animal behavior can be assessed using this combination strategy involving drug delivery followed by imaging.

Many constraints are placed on the valve to meet the specifications for this neuroimaging paradigm. First, our target animal is the transgenic mouse in which many disease models are available. Due to the lack of small form factor valves, the prior system was demonstrated in rats which are much larger than mice (350 g vs. 40 g). The rat pump weighed 32.5 g (\sim 10% of the rat's weight) which was largely due to the solenoid valve and battery required to operate it. By using a microfabricated electrothermal valve, a pump weighing only 2.5 g was possible and suitable for use in mice. This weight requirement also impacts the overall power budget. The target system weight does not allow for a battery, thus wireless approaches were necessary. Furthermore, the low power coupling in air of the wireless system¹² necessitates low power consumption (\sim mW). To minimize diffusion and nonspecific labeling, the valve must open immediately (\sim ms) and contribute minimal fluidic resistance to allow rapid radiotracer release. Finally, after the valve is opened, no valve debris should enter the blood stream or obstruct flow. Therefore, in this study, a microelectromechanical systems (MEMS)-based valve was designed to specifically target these requirements.

Design

The electrothermal valve consists of either two-layer (metal/Parylene) or sandwiched (Parylene/metal/Parylene) thin film composite membranes (Fig. 1(a)–(c)). The metal layer contains a resistive element and was deposited on flexible Parylene membranes. In some versions, an additional overlying Parylene layer was added. The thin film Parylene resists loading by the pressure source (drug reservoir) and supports the thin film metal structures while the resistive metal element, once energized, melts the Parylene membrane and opens the valve. Parylene was selected as the membrane material for its mechanical flexibility

^aMing Hsieh Department of Electrical Engineering, University of Southern California, Los Angeles, CA, 90089, USA

^bDepartment of Biomedical Engineering, University of Southern California, Los Angeles, CA, 90089, USA. E-mail: ellis.meng@usc.edu; Fax: +1-213-821-3897; Tel: +1-213-740-6952

^cDepartment of Psychiatry, Neurology, Cell and Neurobiology, University of Southern California, Los Angeles, CA, 90033, USA

Table 1 Comparison of the Parylene electrothermal valve with one-shot valves reported in research literature

	Bejjed <i>et al.</i> ¹	Liu <i>et al.</i> ²	Aracil <i>et al.</i> ⁵	Griss <i>et al.</i> ⁴	Beebe <i>et al.</i> ³	Maloney <i>et al.</i> ⁶	Luo <i>et al.</i> ⁷	Our Device
Membrane or Plug Materials	Solder Paste	Paraffin	PET ^a	Microsphere	Hydrogel	Pt/Ti/Pt	PMMA ^b	Parylene
Valve Dimension L × W × T (μm)	420 × 420 × N/A	1000 × 500 × N/A	N/A × N/A × N/A	200 × 50 × N/A	300 × 700 × 50	50 × 50 × 0.01	500 × 500 × 100	ø500 × (2, 10, or 20) (thick)
Thermal Element Materials	Cu/Ti	Phenolic Resistor	Au	Transistor	N/A	Pt/Ti/Pt	Au	Pt or Ti
Thermal Element Thickness (Å)	200000/2000	N/A	ø25000	N/A	N/A	10/100/10	10000	2000, 5000, 7500, or 10000
Mass Transport Mechanism	Pressure Driven	Pressure Driven	Pressure Driven	Pressure Driven	Pressure Driven	Diffusion	Diffusion	Pressure Driven
Max. Pressure (kPa (psi))	10000.0 (1450)	275.8 (40)	N/A	100.0 (14.5)	N/A	N/A	N/A	689.4 (100)
Melting Temperature (°C)	137	70	N/A	70	N/A	1770	490	290
Opening Power (mW)	13000	200	N/A	3000	N/A	2250	67	30
Applied Voltage (V)	29.2	3	N/A	N/A	N/A	N/A	2.8	6
Applied Current (mA)	439	N/A	500	N/A	N/A	1000	N/A	4
Valving Time (ms)	3000	20000	N/A	180000	8000	0.01	15000	66
Energy (mJ)	47400	4000	N/A	540000	N/A	0.025	1005	1.98
Biocompatible Construction	No	Yes	No	No	No	Yes	No	Yes
Delivered Material (Solid/Liquid/Gas)	Gas	Liquid	Liquid	Liquid	Liquid	Solid/Liquid	Liquid	Liquid

^a PET is the abbreviation of polyethylene terephthalate. ^b PMMA is the abbreviation of polymethylmethacrylate.

(Young's modulus ~ 4 GPa), biocompatibility (USP class VI material) and compatibility with microfabrication.^{13–15}

The five different resistive elements share a common Ω -shaped geometry but have different element line widths (Table 2). In these designs, a tongue-like flap was included in the metal layer; the purpose of this structure is to strengthen the fold in the Parylene film formed when the freed membrane flap is bent back by the escape of the pressurized contents of the gated fluid reservoir. Fig. 1(d) and (e) demonstrate the valve operation process. Power is transmitted from an activated external primary coil to a secondary coil connected to the valve. Then, current passes through the resistive element and generates Joule heating to melt the adjacent Parylene surrounding the element. The element is designed such that Parylene is melted in a narrow region through part of the circumference of the cannula lumen. Thus, the remainder of the Parylene film is pushed away by the fluid, folding back against the cannula. This piece is supported by a metal-strengthened flap which prevents the Parylene film from washing away or obstructing the fluidic path. Compared to previous electrothermal valves,^{16,17} this improved design requires melting of only the limited Parylene area surrounding the resistive element (instead of melting of the whole valve area) which contributes to a decrease in the power consumption and an increase in the valve opening speed.

Theory and modeling

The valve opening process is achieved through heat transfer from the resistive heating element to the valve membrane material. The mechanical strength of the resistive element plays an important role in valve operation and it must withstand the thermally-induced stress from its supporting membrane during the opening process. Previously, we modeled the mechanical performance of a similar Parylene valve with a different resistive element pattern and demonstrated the mechanical robustness of this Pt resistive element under 1 atm of applied pressure.¹⁶ In this study, two finite element models (FEM) were developed to evaluate heat transfer and thermal stress in our electrothermal valves. First, two transient FEM thermal simulations each with different resistive element geometries were studied for the purpose of improving valve opening by optimizing the heat transfer path to the membrane material. The mechanical performance of the improved valve geometry was further investigated by varying dimensions in six FEM thermal stress simulations.

Thermal modeling

Four major heat transfer routes exist from the resistive element: (1) to the electrical leads, (2) to the Parylene membrane, (3) through the Parylene membrane into fluid (air or water), and (4) through the Parylene membrane into the cannula (Fig. 2(a) and (b)). To simplify the discussion, route 1 and 4 are omitted due to the separation distance and thermal conductivity of these thermal sinks. Route 2 is defined as the heat propagation within the valve membrane and is the critical heat transfer route for valve opening. However, this horizontal heat transfer path (x -direction) within the membrane is much longer than route 3 in the vertical propagation direction (z -direction, radius of

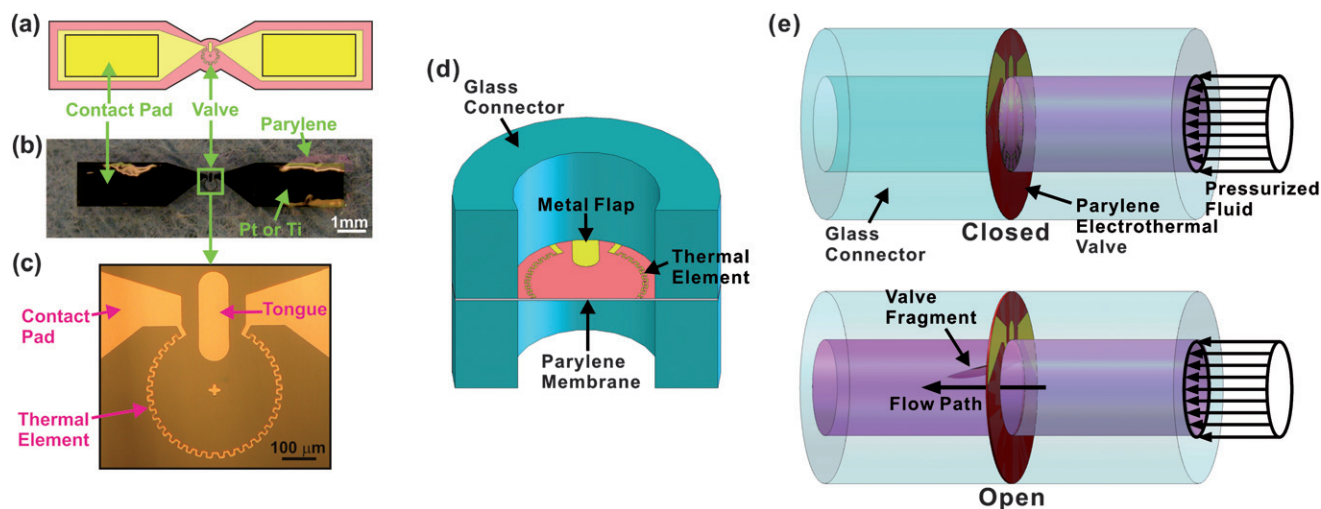


Fig. 1 Schematics and photographs of the Parylene electrothermal valve showing (a) the electrothermal valve layout, (b) a single fabricated valve, (c) close-up of a valve element, (d) cross-sectional view of the valve assembly, and (e) illustration of valve operation.

membrane compared to thickness of membrane). If a high thermal conductivity fluid (relative to the thermal conductivity of Parylene, *e.g.* water) is used, most of the heat will flow into this fluid. Under these conditions, opening the valve requires a much higher input power. However, higher applied power may induce larger membrane deformation and increase the risk of element fracture before valve opening.

Melting of the entire valve area has been a common valve opening strategy in previous electrothermal valve designs.^{6,7,16,17} However, higher heat and power are required and the thin film resistive element may fracture prematurely. Modifying the resistive element design such that it is constrained to the perimeter of the valve area, minimizes the area over which heat transfer is necessary to open the valve and lowers the overall power consumption.

These factors are evident in transient thermal FEM simulations (COSMOSWorks 2007, SolidWorks Co., Concord, MA) that were performed. Two electrothermal valve designs with the same Parylene membrane and different resistive element geometries (A: a serpentine element trace patterned over the entire valve area, and B: an Ω -shaped trace limited to the perimeter of the valve) were investigated (Fig. 2(c) and (d)). The simulation parameters are listed in Table 3. The same power was applied to both elements and air was used as the contact medium. Valve opening occurs when the Parylene membrane temperature is greater than the melting point. Valve A opened after ~ 400 ms and valve B melted in less than 13.3 ms. By 133 ms, valve B reached a stable temperature distribution while the temperature of valve A was still increasing at 400 ms. In addition, a narrow temperature distribution pattern was observed for valve B. As described in the design section, this Ω -shaped element melts only a small quantity of Parylene instead of melting of the entire valve area. Therefore, based on these simulations, the later design strategy was selected for reduced power consumption and faster valve opening.

Thermal stress modeling

Thermal stress modeling was performed on six valve designs having Ω -shaped elements (COSMOSWorks 2007, SolidWorks

Co., Concord, MA). Valves differed in wire style (straight or serpentine), element material (Pt or Ti), wire width ($5\ \mu\text{m}$ or $20\ \mu\text{m}$), and wire thickness ($1000\ \text{\AA}$ or $3000\ \text{\AA}$) (Table 4). In these simulations, electrical power was applied to the resistive traces ($40.5\ \text{mW}$) and the corresponding thermal-induced stress distributions over the entire valve area were obtained (Fig. 3). The maximum thermal stresses in the traces of each valve design are summarized in Table 4. Valve 4 (straight, Ti, $20\ \mu\text{m}$ wide, and thick $3000\ \text{\AA}$ wire) possessed the lowest thermal stress ($276.2\ \text{MPa}$). In general, lower thermal stresses were present in designs with straight traces. The results suggest that mechanically robust traces are dependent on mechanical properties of the metal and the layout geometry (straight, wider, and thicker traces are preferred). Although the FEM software cannot simulate dynamic stresses that occur during the valve melting and opening, these simpler thermal stress simulations can suggest improvements to the overall design.

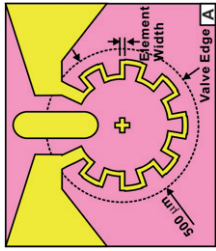
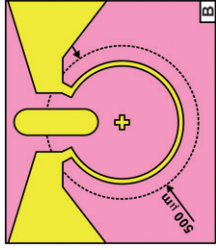
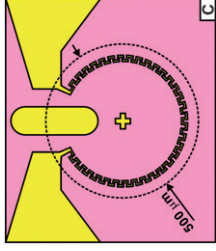
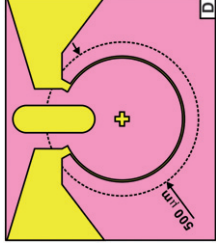
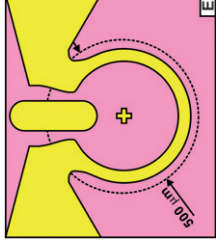
A compromise exists between applied power and valve opening performance. While a faster opening may be desired, high applied power risks premature element fracture before complete valve opening. Air was used as the contact medium in the simulations. However, if water or other liquids are applied instead, a higher applied power will be required to open the valve. In both cases, higher power is associated with an increase in temperature. The elevated temperature induces large deformation of the Parylene membrane and high stress on the thin metal film that may result in premature fracture.

Fabrication

Valve membrane fabrication

Two electrothermal valves consisting of Parylene/metal or Parylene/metal/Parylene layers were constructed using a surface microfabrication process similar to that reported by Li *et al.*^{16,17} First, the bottom Parylene C layer was deposited on a 3 inch silicon wafer with native oxide; the oxide layer facilitates Parylene release at the end of the process. Following lithography, metal (Pt or Ti) was e-beam evaporated. Then the resistive

Table 2 Valve design parameters

Valve ID	A	B	C	D	E
Layout					
Occupied Diameter (μm)	450	450	450	450	450
Element Line Width (μm)	20	20	5	5	40
Total Element Length (μm)	1312	1152	1878	1178	1100
Element Style	Serpentine	Circular	Serpentine	Circular	Circular
Element Corner Geometry	Square	Square	Square	Square	Rounded

element and contact pad were revealed by liftoff. In the case of the Parylene/metal/Parylene construction, another layer of Parylene was deposited and the contact pads were opened using reactive ion etching (O_2 plasma). Valves were manually diced using a fine blade and peeled off the silicon substrate.

Valve packaging

Briefly, a valve was aligned and attached to two short glass tubes (length of 5 mm and inner diameter of 1.0 mm) using laser-machined double-sided adhesive rings (Fig. 4(a)). Electrical wires were joined to the contact pads using conductive epoxy (Fig. 4(b)), and a bead of epoxy was applied at the joint to support the assembly (Fig. 4(c)). Silicone rubber segments (Silastic Laboratory Tubing, Dow Corning, Midland, MI) were connected to the ends of the glass tubes (Fig. 4(d)). Finally, the entire joint was encapsulated with silicone prepolymer (Sylgard 184, Dow Corning, Midland, MI) and cured at 65 °C for one hour (Fig. 4(e)). The assembly process was performed under a stereo microscope.

Experimental methods

Valve opening performance under various experimental conditions was investigated: material and fabrication (element ID and valve structure), contact medium, mechanical conditions (applied pressure), and electrical conditions (applied current and thermistor). Five resistive element patterns (Table 2) and four valve structures with different metals and Parylene thicknesses were tested (Table 5). Both air and water were used as contact medium. Some valves were operated under pressurized conditions (200 mmHg) to evaluate their mechanical robustness. Three biasing modes (constant current, current ramping, and wireless) and the use of a series thermistor as an inrush current limiter, were investigated to determine their effect on valve opening performance. Initial experiments were first conducted on freed valves using a custom testing fixture that facilitated control of the contact medium and applied pressure. Then, testing of fully packaged valves was performed.

Valve opening experiments in test fixtures

Custom testing fixtures were laser-machined (Mini/Helix 8000, Epilog, Golden, CO) in acrylic; this fixture allowed control of both electrical connections and mechanical pressure loading such that conditions similar to those imposed on a valve in the actual drug delivery application were easily replicated (Fig. 5). The experimental conditions are listed in Table 5. The valve opening process was monitored using a compound microscope and computer-controlled CCD camera (PL-A662, PixeLINK, Ottawa, Canada) system. As listed in Table 5, this testing apparatus allowed application of mechanical and electrical conditions including: (1) contact medium (water or air) on the bottom side of the valve (2) pressure (200 mmHg), and (3) biasing using a DC power supply or a custom RF inductive power transfer system (2 MHz) specifically developed for biomedical implants.¹² This RF system includes an external 5-turn primary coil (20 cm diameter) and an implanted 5-turn, 1.3 cm diameter Litz-wire secondary coil. A class E oscillator was chosen for the transmitter because it achieves much higher efficiency than

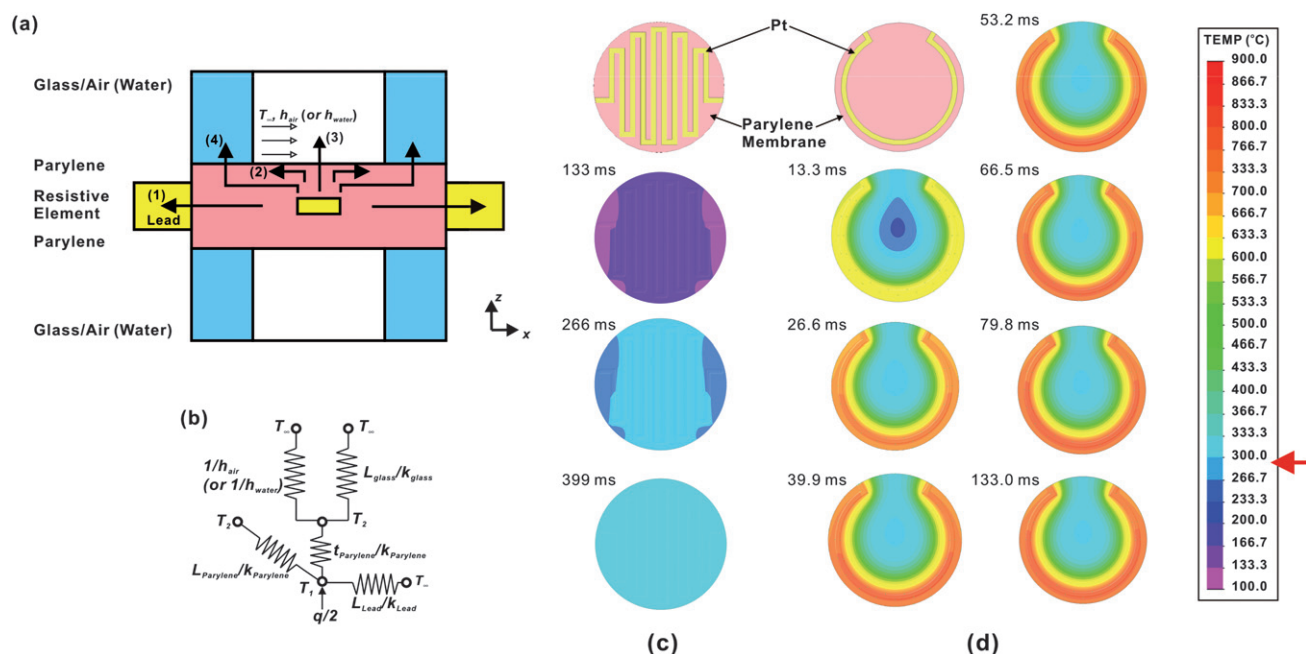


Fig. 2 Thermal modeling: (a) a schematic diagram showing a 2-D heat transfer model with arrows indicating the heat propagation routes, and (b) an equivalent thermal resistance circuit model. Transient thermal FEM using COSMOSWorks comparing the temperature distributions of (c) a valve with a serpentine trace covering the entire valve area and (d) a valve with an Ω -shaped trace occupying only the perimeter of the valve. For (b), h is the convective heat transfer coefficient, T is the temperature, L is the material thickness, and q is the heat generated by the resistive element. Only the top half of the valve is used due to the symmetry. The step time is 133 ms for (c) and 13.3 ms for (d). The arrow on the temperature scale indicates the melting temperature of Parylene (290 °C).

Table 3 Parameters used in transient thermal FEM

Valve Properties or Parameters	Previous Valve	Current Valve
Applied Electrical Power (mW)	40.5	40.5
Material of Resistive Element	Platinum	Platinum
Width of Resistive Element (μm)	20	20
Geometry of Resistive Element	Serpentine	Ω -shaped
Trace Route of Resistive Element	Whole Valve Area	Valve Perimeter Only
Material of Valve Membrane	Parylene	Parylene
Thickness of Valve Membrane (μm)	10	10
Diameter of Valve Membrane (μm)	500	500

Table 4 FEM thermal stress results of thermal elements having different styles, materials, widths, and thicknesses

Valve	Valve ID	Element Material	Element Width (mm)	Pt Thickness (\AA)	Max Thermal Stress (MPa)
1	A	Pt	20	1000	493.0
2	A	Pt	20	3000	438.0
3	B	Pt	20	3000	351.2
4 ^a	B	Ti	20	3000	276.2
5	C	Pt	5	3000	725.0
6	D	Pt	5	3000	553.6

^a The optimal design.

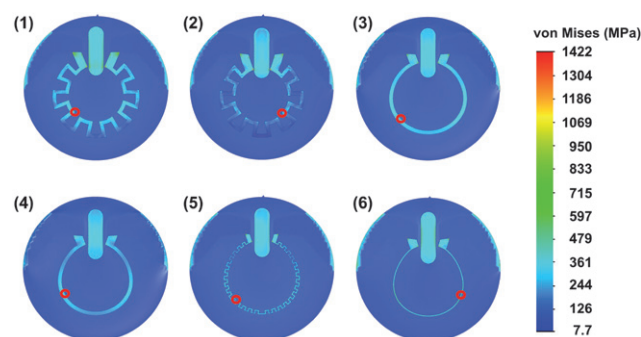


Fig. 3 FEM thermal stress analysis of resistive elements having different styles, materials, widths, and thicknesses as listed in Table 4. The maximum stress sites are circled. The original corresponding patterns were shown in Table 2.

conventional class B or C amplifiers. The biasing circuits are summarized in Fig. 5(c) and include constant current biasing (2400 SourceMeter, Keithley Instruments Inc., Cleveland, OH) with or without a series thermistor (SM103J1K, US Sensors, Orange, CA), and wireless powering with or without a series thermistor. In RF experiments, a resistor was first connected to acquire the root-mean-squared (RMS) voltage using an oscilloscope (AFG3021, Tektronix, Inc., Beaverton, OR). The associated RMS current could then be calculated.

Packaged valve opening testing

The opening performance of packaged valves connected to a drug reservoir was investigated (Table 5 and Fig. 5(b)). Here,

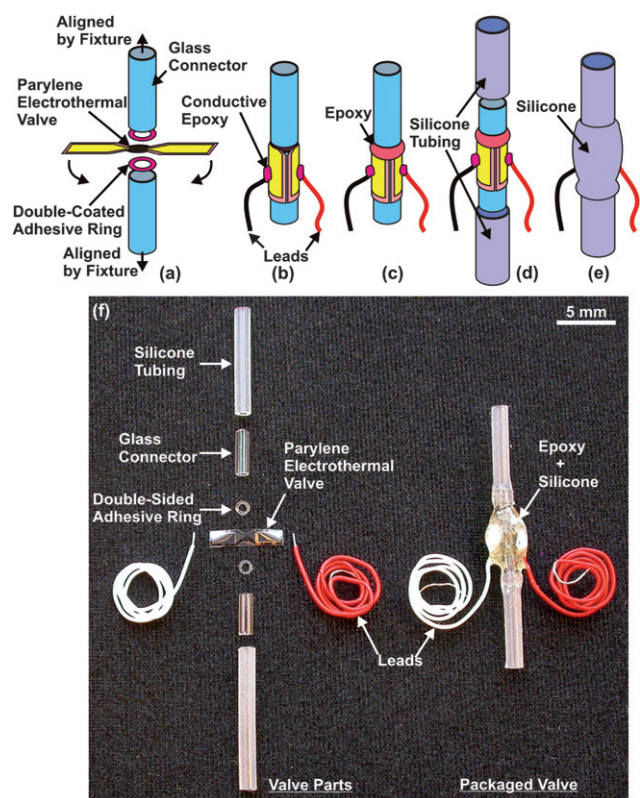


Fig. 4 Illustrated assembly process for the Parylene electrothermal valve: (a) exploded view of components, (b) sandwiched valve with electrical leads, (c) epoxy encapsulation, (d) addition of silicone tubing for connection to drug pump, and (e) silicone encapsulation of entire valve assembly. Photograph (f) showing components for the valve (left) and a packaged valve with silicone tubing (right).

three valve structures were tested. Constant current or RF power were applied; the thermistor was used in one experiment. The drug reservoir was pre-pressurized with DI water to 200 mmHg. Experiments were conducted with or without an air pocket between the valve and fluid contained in the reservoir.

Results and discussion

Valve opening experiments in test fixtures

Four valve structures clamped in test fixtures were tested under twenty one experimental conditions (conditions 1–21) and the results are summarized in Table 5. Valve designs were improved through careful design followed by experimental validation in order to achieve the goal of low power operation of valves exposed to pressurized liquid. First, devices having the new refined Ω -shaped geometry were tested in air (Pt (2000 Å)/Parylene (2 μm) and conditions 1–4 in Table 5). As expected, valves were opened successfully and consistent opening currents were obtained for each of the resistive element patterns (A–D). The typical opening time was <1 s; with the fastest at \sim tens of ms (Fig. 6(a)), which was in close agreement with thermal FEM results (Fig. 2(d)). Higher applied current can decrease further the opening times. However, sufficiently large applied currents induced significant thermal stress in excess of the mechanical strength of the resistive elements. Consequently, resistive

elements fractured instantly before complete valve opening; this was a common failure mode. As expected, the maximum opening current for patterns B and D (straight) was higher than A and C (serpentine).

Successful valve opening was more difficult when water was the bottom medium (conditions 5–20). Water was introduced below the valve but not on the top in order to easily assess the valve condition with a compound microscope; in select cases, water was also introduced on the top side (conditions 14 and 18). As expected, higher currents were necessary to open the valve in water. In initial experiments with Pt/Parylene devices (conditions 5–8), we observed instantaneous fracture of the resistive elements under high currents before complete valve opening. Only one valve opened using constant current biasing of 20 mA. Therefore, an improvement of valve design was required.

Several approaches were investigated to improve valve performance for the intended application, with focus on the appropriate balance between low power operation, valve mechanical strength, and optimal heat transfer. First, fracture of the metal trace was addressed by changing the geometry of the trace (thicker and wider) and the metal (from Pt to Ti). These modifications were supported by thermal FEM simulations (Fig. 3). In subsequent experiments described later, delamination of the metal trace was identified as a failure mode (Fig. 6(c), condition 9). A top layer of Parylene was added or made thicker to better support the metal element. As reported previously,^{16,17} constant current biasing may also induce premature failure of the metal trace prior to valve opening due to the initial current spike. Instead, constant rate current ramping was used to successfully trigger valve opening in the presence of water (condition 10). This approach was associated with a significant increase in opening time and required complex circuitry. So, variable rate current ramping was implemented by simply including a series thermistor as an inrush current limiter (conditions 13, 14, and 16–19).

After changing the metal from Pt to Ti and increasing the thickness, delamination in addition to fracture was observed in metal structures following current application (Fig. 6(c), condition 9). Even when applying a constant rate current ramp, some valves failed in the same manner (condition 10). The large difference in the coefficients of thermal expansion between Ti and Parylene (8.8×10^{-6} vs $35 \times 10^{-6} \text{ K}^{-1}$) may contribute to the detachment but the cause of failure is not well understood. However, in comparison to the thinner Pt elements, these Ti elements survived higher currents indicating that increased metal thickness improved fracture resistance.

A simple solution to prevent detachment was to deposit an additional layer of Parylene (8–10 μm) on top of the otherwise open metal pattern (conditions 11–21). Valves were successfully opened under constant current in water (condition 11) but not when pressure was applied (200 mmHg, condition 12). Also, valves with thicker Parylene did not open consistently in water (condition 15). Given the prior success with current ramping, a thermistor was connected in series to provide variable rate current ramping and limit inrush current. First, thermistors were calibrated to confirm a suitable variation of resistance over time at different currents; note that in the target application, rapid opening is required (Fig. 7). Variable rate current ramping successfully opened valves with and without pressure that had thicker Parylene and wider metal traces (Fig. 6(b), conditions

Table 5 Parameters used in the investigation of the valve opening performance using a test fixture

Experimental Condition	Valve Structure and Material				Medium		Applied Pressure (mmHg)	Applied Current Mode ^b	Thermistor	Package	Number of Valves Tested	Number of Valves Opened	Typical Valve Opening Results ^c	Typical Resistive Element Performance ^d	Valve Opening Currents (mA) or Current Ramping Rate (mA/sec)
	Valve ID ^a	Bottom Parylene	Metal	Top Parylene	Bottom	Top									
1	A	2 µm	Pt (2000 Å)	N/A	Air	Air	0	CC	No	No	9	8	O or X	S or B	25.0–30.0
2	B	2 µm	Pt (2000 Å)	N/A	Air	Air	0	CC	No	No	6	5	O or X	S or B	25.0–32.5
3	C	2 µm	Pt (2000 Å)	N/A	Air	Air	0	CC	No	No	6	5	O or X	S or B	7.5–12.5
4	D	2 µm	Pt (2000 Å)	N/A	Air	Air	0	CC	No	No	7	6	O or X	S or B	7.5–15.0
5	A	2 µm	Pt (2000 Å)	N/A	Water	Air	0	CC	No	No	2	0	X	B	N/A
6	B	2 µm	Pt (2000 Å)	N/A	Water	Air	0	CC	No	No	2	0	X	B	N/A
7	C	2 µm	Pt (2000 Å)	N/A	Water	Air	0	CC	No	No	2	1	O or X	S or B	20
8	D	2 µm	Pt (2000 Å)	N/A	Water	Air	0	CC	No	No	2	0	X	B	N/A
9	A	2 µm	Ti (5000 Å)	N/A	Water	Air	0	CC	No	No	6	0	O– or X	S or D	N/A
10	A	2 µm	Ti (5000 Å)	N/A	Water	Air	0	CR	No	No	3	1	O, O–, or X	S or D	1.67 (CR)
11	A	2 µm	Ti (10000 Å)	8 µm	Water	Air	0	CC	No	No	4	4	O	S	30
12	A	2 µm	Ti (10000 Å)	8 µm	Water	Air	200	CC	No	No	2	0	X+ or X	S or B	N/A
13	A	2 µm	Ti (10000 Å)	8 µm	Water	Air	200	CC	Yes	No	3	0	O–/P or X	S or B	N/A
14	A	2 µm	Ti (10000 Å)	8 µm	Water	Water	200	CC	Yes	No	2	0	X	B	N/A
15	E	10 µm	Ti (7500 Å)	10 µm	Water	Air	0	CC	No	No	5	1	O, O– or X	S or B	40
16	E	10 µm	Ti (7500 Å)	10 µm	Water	Air	0	CC	Yes	No	5	4	O or OX	SB	35
17	E	10 µm	Ti (7500 Å)	10 µm	Water	Air	200	CC	Yes	No	7	3	O, XP, or X	S or B	38 and 50
18	E	10 µm	Ti (7500 Å)	10 µm	Water	Water	200	CC	Yes	No	5	0	O–/P or X+/P	SB	N/A
19	E	10 µm	Ti (7500 Å)	10 µm	Water	Water	200	RF	Yes	No	1	0	LP	N/A	N/A
20	E	10 µm	Ti (7500 Å)	10 µm	Water	Air	200	RF	No	No	1	0	O–/P	S	N/A
21	E	10 µm	Ti (7500 Å)	10 µm	Air	Air	200	RF	No	No	1	1	O	S	39 ^e
22	C	2 µm	Pt (2000 Å)	N/A	Water & Air Pocket	Air	200	CC	No	Yes	5	1	O or X	S or B	27.5
23	C	2 µm	Pt (2000 Å)	N/A	Water Pocket & Air	Air	200	RF	No	Yes	2	0	O– or X	S or B	N/A
24	A	2 µm	Pt (2000 Å)	7 µm	Water	Air	200	CC	No	Yes	2	0	X	S	N/A
25	E	10 µm	Ti (7500 Å)	10 µm	Water	Air	200	RF	Yes	Yes	1	0	LP	N/A	N/A
26	E	10 µm	Ti (7500 Å)	10 µm	Water & Air Pocket	Air	200	RF	No	Yes	4	1	O or X+/P	S	58 ^e

^a See Table 2 for key. ^b CC: constant current, CR: current ramping, and RF: radio frequency power transfer. ^c O: valve opened successfully, O–: valve opened partially, X+: small opening hole formed, X: valve did not open, P: Parylene balloon, and LP: insufficient power to open. ^d B: element broke instantly, S: element broke during operation, and D: element broke instantly and detached from valve membrane. ^e This power was estimated using a series resistor with the same resistance as the valve immediately before the opening experiment.

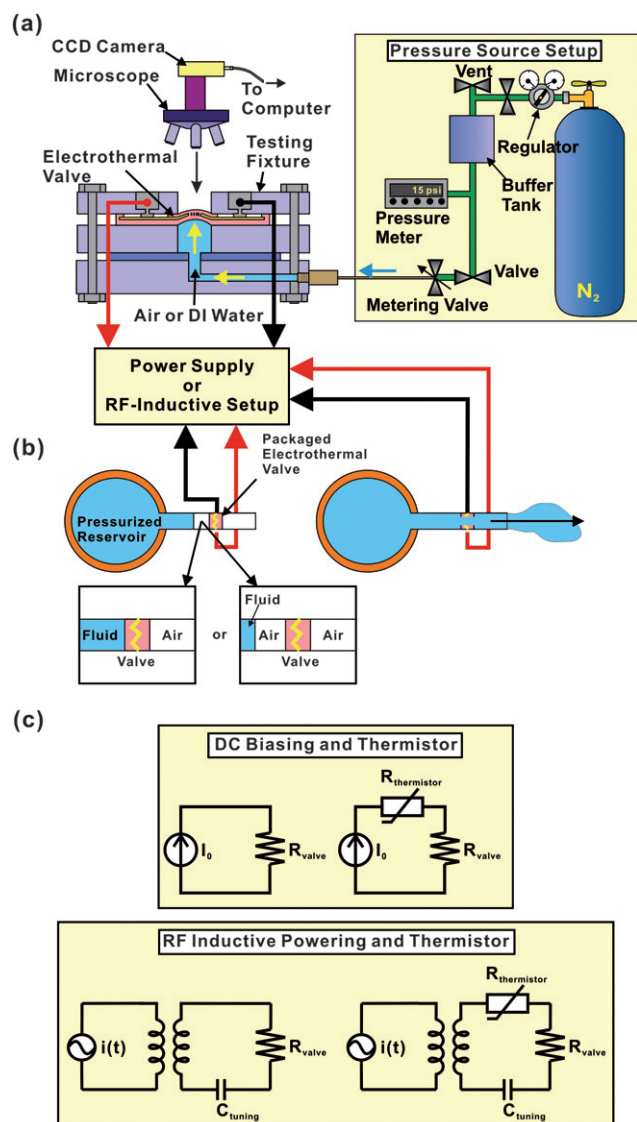


Fig. 5 Schematics of the valve opening experimental setups: (a) universal test fixture for unpackaged valves, (b) testing setup for packaged valves (an optional air pocket may be inserted on the pressurized side), and (c) circuit diagrams illustrating the valve electrical connections with or without a series thermistor in both DC and RF operation modes.

16–17) but not thinner Parylene (condition 13). Interestingly, thinner valves experienced incomplete opening due to the formation of a Parylene balloon (Fig. 6(d)). The permanent balloons were formed as the valve membrane began to melt. Softened Parylene inflated under pressurized conditions causing the trace to fracture. Without Joule heating, the balloon cooled quickly in the presence of water. Thicker valve membranes and wider traces provided sufficient mechanical support to metal traces to allow complete opening prior to metal fracture, although some Parylene balloons were still observed. In these strengthened devices, the Ti thickness was decreased to maintain similar resistance values.

In two experiments (conditions 14 and 18), water was introduced on both sides of the valve. Both valves experienced instant trace fracture and Parylene balloons as failure modes due to the increased current. Significant heat transfer from the valve to the

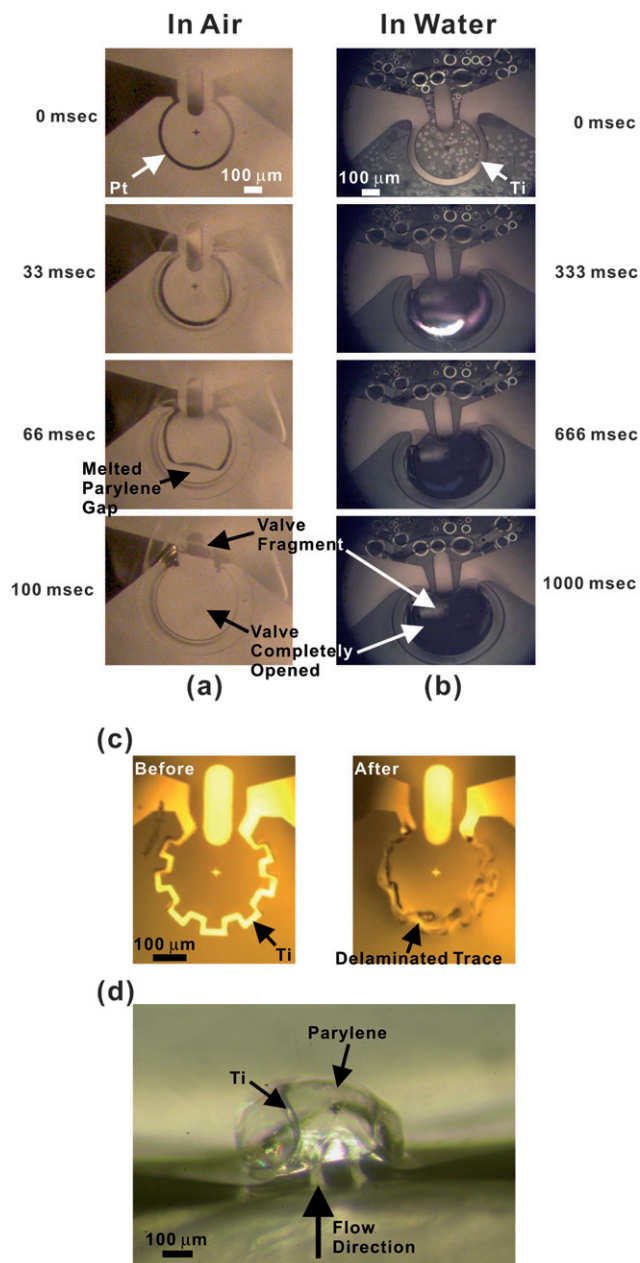


Fig. 6 Microscope images showing (a) sequential images of a valve opening for a Pt (2000 Å)/Parylene (2 μm) valve under a constant current of 32.5 mA in air and (b) for a Parylene (10 μm)/Ti (7500 Å)/Parylene (10 μm) valve under 50 mA in water. (c) Before and after images of a valve element that delaminated after application of constant current. (d) Side view of a Parylene balloon formed by cooling of the membrane due to fracture of the metal element and heat transfer into water.

surrounding medium limits valve application to cases in which air or a small air pocket can be tolerated on one side.

Finally, RF operation of valves was examined (Fig. 5(a), conditions 19–21). Operation was successful for pressurized air (condition 21) but not water (conditions 19–20). The water experiments were performed with (condition 19) and without a series thermistor (condition 20). Due to the finite power consumption of the thermistor, the wireless system was unable to supply enough current to trigger the valve. Without the

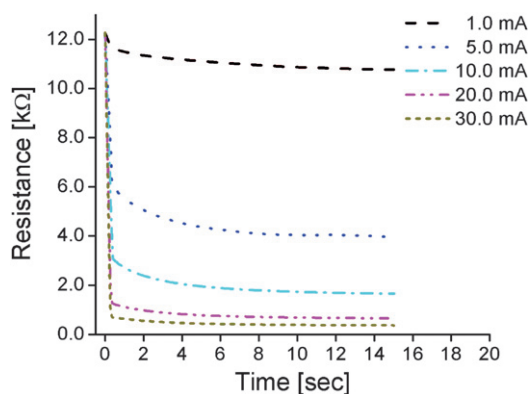


Fig. 7 Thermistor calibration in which the real-time resistance drop under different applied currents was measured. The variable resistance allows a current ramp to be applied to the valve.

thermistor, partial valve opening and a Parylene balloon was observed. Thus, for practical operation with the current wireless system, air pockets need to be introduced on both sides of the valve (1–20 μL) to separate the water from contacting the valve. However, increasing the RF power is preferred and will also be pursued to accommodate a series thermistor.

Packaged valve opening testing

Completely packaged valves were evaluated and a total of three valve layouts were tested (Table 5 and conditions 22–26). Pressurized valves with Pt and thinner Parylene did not open except in one case which was consistent with the results for the unpackaged valves (Fig. 5(b), conditions 22–24). Valves having thicker Parylene were operated under RF power transfer (Fig 5(b)). With a series thermistor, again the power supplied was insufficient to open the valve (condition 25). Successful wireless operation of a completed packaged valve was achieved when an air pocket was introduced between the valve and pressurized water (condition 26). In total, four valves were tested wirelessly with different RMS currents and an air pocket volume (1 or 20 μL). These RMS currents were estimated prior to valve operation through a load resistor and the associated currents were calculated. For a 1 μL air pocket, three valves were tested but none of them opened. The Ti trace remained intact until the pressurized water contacted the valve at which point the valve cooled instantly, the trace fractured, and a Parylene balloon formed. By increasing the air pocket to 20 μL , complete valve opening was obtained (58 mA) and the pressurized water rapidly flowed through the valve. This air pocket volume allowed sufficient time for the valve to open before contact with pressurized water. However, 20 μL of air may not be tolerated by the mouse circulatory system and an air embolus may occur. Therefore, based on the previous results, increasing the wireless system's power to accommodate the thermistor will allow optimal operational conditions for the current valve without requiring the presence of air pockets.

Neuroimaging application

Our Parylene electrothermal valve is an integral component of the mouse infusion pump (MIP) that gates radiotracer release in

a real-time *in vivo* neuroimaging application. The wireless activation of the valve was achieved using a custom RF inductive power transfer system. This system will be further improved in order to power a series thermistor and the valve. Then preliminary animal implants will be performed followed by neuroimaging experiments. The neuroimaging approach is briefly summarized here. A pump is implanted into the animal. Following recovery, animal behavior is monitored and when the targeted behavioral event occurs, an RF signal is transmitted wirelessly to activate the valve and rapidly infuse radiotracer followed by euthanasia agent. Finally, the brain is removed, sliced, and imaged using autoradiographic processing of labeled tissue slices to obtain a 3-D reconstructed statistical parametric mapping.

Freely-moving animals will vary their location as well as their position in these planned experiments. Thus, the wireless activation system must be able to activate the valve regardless of animal position and location within the testing cage. In our previous study in freely-moving rats, we demonstrated wireless activation of an electromagnetic valve.^{10–12} Therefore, RF power coupling to different orientations and locations of the implanted coil is expected to be adequate for our future experiments in mice.

Conclusion

We developed a low power, on demand Parylene MEMS electrothermal valve suitable for implantable drug delivery and biological fluid handling applications. The Ω -shape resistive element melts only a small portion of the valve membrane which decreases the power consumption and increases the valve opening speed. A metal flap was incorporated to strengthen the folded valve membrane and prevent debris from entering the blood stream. FEM thermal modeling predicted a higher temperature increase rate for the Ω -shape resistive element compared to a serpentine design that spanned the entire valve area. Thermal stress FEM indicated wider and thicker traces with rounded corners improved mechanical robustness. Valves were fabricated using a simple process and packaged with minimal dead volume. Operation was demonstrated in both air and water, with or without pressure. Through FEM and experiments, a robust valve was obtained and optimal operating conditions were determined. Failure modes were identified and addressed. A series thermistor improved the valve opening by optimizing heat transfer. Successful wireless valve operation was demonstrated.

Acknowledgements

This work was supported in part by the NIH/NINDS (1 R01 NS050171). The authors would like to thank Dr Donghai Zhu, Dr Tuan Hoang, and members of the Biomedical Microsystems Lab at the University of Southern California for their contributions to this work.

References

- 1 J. Bejhed, P. Rangsten and J. Kohler, *J. Micromech. Microeng.*, 2007, **17**, 472–481.
- 2 R. H. Liu, J. Bonanno, J. Yang, R. Lenigk and P. Grodzinski, *Sens. Actuators, B*, 2004, **98**, 328–336.

-
- 3 D. J. Beebe, J. S. Moore, J. M. Bauer, Q. Yu, R. H. Liu, C. Devadoss and B.-H. Jo, *Nature*, 2000, **404**, 588–590.
 - 4 P. Griss, H. Andersson and G. Stemme, *Lab Chip*, 2002, **2**, 117–120.
 - 5 C. Aracil, J. Garcia and J. M. Quero, *Industrial Electronics*, 2007. *ISIE 2007*. IEEE International Symposium on, 2007.
 - 6 J. M. Maloney, S. A. Uhland, B. F. Polito, J. N. F. Sheppard, C. M. Pelta and J. J. T. Santini, *J. Controlled Release*, 2005, **109**, 244–255.
 - 7 C. Luo, X. Liu, R. Poddar, G. John, A. P. Gadre, E. V. Keuren, T. Schneider, R. White, J. Currie and M. Paranjape, *J. Micromech. Microeng.*, 2006, **16**, 580–588.
 - 8 A. M. Cardenas-Valencia, J. Dlutowski, J. Bumgarner, C. Munoz, W. Wang, R. Popuri and L. Langebrake, *Sens. Actuators, A*, 2007, **136**, 374–384.
 - 9 K. W. Oh and C. H. Ahn, *J. Micromech. Microeng.*, 2006, **16**, R13–R39.
 - 10 D. P. Holschneider, J.-M. I. Maarek, J. Harimoto, J. Yang and O. U. Scremin, *Am. J. Physiol.*, 2002, **283**, H1713–H1719.
 - 11 D. P. Holschneider and J. M. I. Maarek, *Methods*, 2008, **45**, 255–261.
 - 12 W. H. Moore, D. P. Holschneider, T. K. Givrad and J. M. I. Maarek, *IEEE Trans. Biomed. Eng.*, 2006, **53**, 1705–1708.
 - 13 E. Meng, P.-Y. Li and Y.-C. Tai, *J. Micromech. Microeng.*, 2008, **18**, 045004.
 - 14 E. Meng, P.-Y. Li and Y.-C. Tai, *Sens. Actuators, A*, 2008, **144**, 18–28.
 - 15 P.-Y. Li, J. Shih, R. Lo, S. Saati, R. Agrawal, M. S. Humayun, Y.-C. Tai and E. Meng, *Sens. Actuators, A*, 2008, **143**, 41–48.
 - 16 P.-Y. Li, T. K. Givrad, D. P. Holschneider, J.-M. I. Maarek and E. Meng, *Solid-State Sensors, Actuators, and Microsystems Workshop*, Hilton Head Island, SC, 2008.
 - 17 P.-Y. Li, T. K. Givrad, D. P. Holschneider, J.-M. I. Maarek and E. Meng, *The 12th International Conference on Miniaturized Systems for Chemistry and Life Sciences*, San Diego, CA, 2008.